CHAPTER 15

Photodynamic Therapy in Bone

Stuart K. Bisland

Introduction

Recent work within our group suggests that the application of photodynamic therapy (PDT) in bone holds considerable promise for a number of key conditions specific to bone, including the treatment of primary and secondary cancers, infection, and skeletal deformity. In this chapter I will provide a synopsis of preclinical results obtained using PDT in bone that starts with an overview of the preclinical testing of PDT using liposome-formulated benzoporphyrin-derivative monoacid (BPD-MA, verteporfin) for treating human breast cancer metastases in the spine. Current treatment planning strategies, intraoperative image guidance and navigation as well as protocols for assessing posttreatment response in vivo are also discussed. Antimicrobial PDT is a growing field and Section 15.2 describes some of our work in a small animal model of osteomyelitis. Results are described for PDT treatment of Staphylococcus aureus and Pseudomonas aeruginosa cultures in vitro and in vivo that highlight the need for PDT regimens that will provide long-term management of obstinate or recurrent infections. The final section of this chapter describes some work examining the effects of PDT on endochondral bone and raises a number of interesting possibilities regarding the potential role for PDT in bone growth modulation.

15.1 Photodynamic Therapy for Spinal Metastases

15.1.1 Spinal Metastases

Almost half of all cancers reported, approximately 1.5 million new cases each year in North America alone, have the propensity to metastasize into bone, in particular the spine. Statistical review regarding the prevalence and incidence of cancers in the United States readers can be accessed online (http://www.cancer.org). Certain primary cancers; breast, prostrate, lung, and thyroid are highly metastatic to spine and account for the majority of the 100,000 patients being treated each year in North America for spinal metastases, each with varying prognoses depending on the primary tumor [1]. A study of 425 patients with spinal metastases determined a 70% survival rate at 1 year for breast cancer, 83% for prostate, 22% for lung, and 0% for gastric [2]. Irrespective of primary tumor, patients with spinal metastases are typically moribund with debilitating pain secondary to osteolysis, fractures, or nerve impingement by the lesion. The subsequent loss of ambulation can lead to

conditions that dramatically impact survival, including pneumonia, bedsores, urinary tract infections, and hypercalcaemia [3–7], emphasizing the importance of quality of life for these patients. The complexity of pathways governing the behavior of cancer cells, bone cells, and progenitor cells are only being realized [8–12] and will be instrumental in the design of therapeutic strategies for the future.

15.1.2 Conventional Therapies

Medical advancements continue to prolong survival for many critically ill patients, prompting a demand for improved palliative therapies that offer maximal pain relief and functional preservation. Current conventional treatments for spinal metastases, including bisphosphonates, radiation therapy, and surgery [13–16] do little toward this goal. Treatments can be expensive and are fraught with complications. For the 10% of patients that present with epidural invasion and neurological compromise, treatment options are traditionally surgery followed by radiation, while treatment for the remaining 90% of patients that do not display neurological compromise remains controversial. Surgery can be conducted via anterior or combined anterior/posterior approach with thoracotomy and/or piecemeal excision of the tumor, and pain control is typically good with neurological recovery and continued ambulation despite the often-protracted recovery times [3–5, 7]. The risks, however, remain significant, with complication rates ranging from 20% to 30% and 1% to 9 % mortality rates at 1 month with mean mortality from 7.5 to 15.9 months [3–5, 7]. Recurrence at the surgical site is a primary cause of failure in as many as 50% of patients following intralesion resection, and preoperative radiation therapy may further increase this [16]. For patients without neurological compromise the argument for radiation therapy is often questionable due to toxicity or tumor resistance [17]. Radiation therapy also offers only partial pain relief (35%), which may be delayed and does nothing to address the bone instability and/or microfractures caused by the tumor [14, 17–19]. In fact, radiation-induced myelopathy can exacerbate instability [16]. Recurrence rates and/or failure rates are also high [19], with secondary complications related to wound dehiscence. Yet despite the poor selectivity of radiation and its related morbidity, the difficulty in defining tumor margins will ensure that preoperative radiation remains part of the standard of care. New targeted methods such as intensity modulated radiation or gamma knife radio-surgery will likely improve clinical outcome. However, the higher costs associated with these technologies currently limit availability.

15.1.3 Photodynamic Therapy

The need for improved interventional approaches for patients with advanced stage spinal metastases led us to consider photodynamic therapy. We hypothesized that placing submillimeter optical fiber(s) into diseased vertebrae would allow selective PDT-mediated tumor ablation without damaging the spinal cord. We further proposed that PDT could be used in combination with vertebroplasty or kyphoplasty to stabilize the bone. Importantly, PDT has been shown to be effective in patients who have failed radiation therapy and is not associated with resistance following repeat treatments [20, 21].

15.1.4 A Model of Human Breast Cancer Derived Spinal Metastases

To demonstrate the proof of principle, we developed a rodent model similar to that described by Engebraaten and Fodstad [22]. Human breast cancer cells, MT-1, were transfected with the luciferase gene, allowing noninvasive bioluminescence monitoring of tumor growth within the bone. A close correlation between tumor burden and bioluminescence signal was found and subsequently confirmed histologically (25). Rats typically developed lesions with quantifiable levels of bioluminescence within 10 to 14 days post intracardiac injection of 2×10^6 MT-1Luc cells (in 200 μL). Lesions were usually discretely localized to bony sites; the spine, femur, humerus, and mandible as well as other soft tissues (lung, liver, and ovaries) [23–25] (Color Plate 16).

Microcomputed tomography images revealed osteolytic degradation of rat vertebrae with mean areas of 2.92 and 2.14 mm^2 in lumbar and thoracic spine, respectively. The clinical manifestations of disease mirrored that in humans with osteolysis, cachexia, and escalating morbidity such that by day 26 postinjection, rats had to be euthanized. The effects of PDT were conclusive. In lumbar spine, an intravenous bolus injection of verteporfin (2 mg/Kg) followed 3 hours later by 690-nm light of 150J via percutaneous placement directly onto the lateral aspect of the target vertebral body, effectively ablated the tumor resulting in a 99.8% decrease in bioluminescence signal within 48 hours. Histology confirmed destruction of normal bone marrow and fat cells resulting in a dose-dependent increase in the area of effect. At 150J, the maximal mean rostal-caudal diameter of effect in lumbar spine (L2) was 13.1 ±2.1 mm and 80.53 mm^2 area (mid-sagittal). The mean mid-sagittal dimensions of vertebrae were 7.1 ±0.8 (rostal-caudal) by 9.4 ±1.1 mm (dorsal-ventral) so treatment area typically spanned 2 to 3 vertebrae (26). Importantly, more than one third of the animals treated in the thoracic spine using the same treatment regimen became paralyzed, confirming the sensitivity of the spinal cord. Thoracic spine is an important target accounting for 70% of spinal metastic cases compared with only 20% in lumbar spine [1], and it will be important for future experiments to establish a safe, effective regimen for this region of the spine. At 3 hours postintravenous injection, Verteporfin is confined largely to the vasculature with the remainder going to liver, kidney, ovaries, and bone marrow (29). Interestingly, the amounts of Verteporfin within vertebrae containing tumor were 3.4-fold that of spinal cord at 3 hours postinjection, which further increased to 5.5-fold at 15 minutes postinjection, suggesting that 15 minutes is better. All subsequent studies were performed with this short drug-light interval. The amount of light that reaches the spinal cord in a human vertebra is expected to be orders of magnitude less than that in the rat primary due to the differences in size; nevertheless, the risk of paralysis highlights the importance of pharmacokinetics in optimizing selectivity.

15.1.5 Optical Dosimetry

Bone is naturally scattering to light, containing 58% inorganic hydroxyapatite crystals, 12% water, 25% collagen, and 5% carbohydrate. However, for dosimetry of trabecular bone it is important to consider the influence of blood and bone marrow as well. Studies to evaluate the optical properties of bone tissues have resulted in

controversy with different values depending on the technique used [26–29]. Common methods of measurement include diffuse reflectance spectroscopy, which allows multiple scattering approximations based on diffusion theory or reflectance and transmittance measurements using integrating spheres [27]. The later typically involves Monte Carlo lookup tables for calculation and requires that samples be prepared as very thin (submillimeter) slices, which for trabecular bone is challenging. Nevertheless, we obtained optical properties for fresh porcine vertebrae of μa = 0.057 ±0.001 mm^{-1} and $\mu s'$ = 1.819 ±0.095 mm^{-1} at 690 nm, which were realistic when compared to those for cortical bone obtained using similar methods, μa = 0.040 ±0.002 mm^{-1}, $\mu s'$ = 2.651 ±0.053 and g = 0.925 ±0.014 nm [27]. Attenuation was reduced to 0.021 ± 0.001 following washout of residual blood. Phantoms studies representing trabecular bone and breast tumor [30] confirmed the accuracy of our measurements to within 2% error at 1.2-cm distance from the delivery fiber based on diffusion theory specific to linear diffusers [31]. Similar results were obtained in vivo [25], although tissue heterogeneity and blood pooling effects around the delivery fiber limited the reproducibility of results. Similar problems are anticipated in patients and will need to be addressed together with the dynamic changes in tissue optical properties that occur during treatment (see below).

15.1.6 PDT Dosimetry

Diffusion theory (15.1) and the finite element method can be used to calculate the fluence rate [W/cm^2] anywhere within a target volume based on tissue optical properties [31, 32]. Fluence rate integrated over treatment time provides the total fluence [J/cm^2] delivered to the tissue, which combined with the concentration of photosensitizer in each tissue type, gives the PDT dose (15.2) throughout the target volume, akin to the reciprocity principle.

$$\nabla D \cdot \nabla \mu_a \phi = 0 \tag{15.1}$$

In (15.1), diffusion theory is where D is the diffusion coefficient, $D = \left[3\left(\mu_a + \mu_s'\right)\right]^{-1}$, ϕ is the fluence rate [W/cm^2], μ_a is the absorption coefficient [cm^{-1}], and μ_s' is the reduced scattering coefficient.

$$Dose = 2.303 \varepsilon C \Phi \frac{\lambda}{1980} 10^{19} \tag{\{(15.2)}$$

where ε is the extinction coefficient of the photosensitizer [cm^{-1} (μg/g)$^{-1}$], C is the photosensitizer concentration in the tissue [μg/g], Φ is the accumulated light energy in the tissue [J/cm^2], and λ is the wavelength of the activation light [nm].

PDT dose is expressed in photons absorbed by the photosensitzer per cm^3 of tissue. Dose-volume histograms, a standard analysis tool in radiation treatment planning, yield quantitative dose statistics for individual structures, such as the percentage of tumor volume that receives a PDT dose greater or equal to the threshold dose required for tumor kill or similarly, the percentage of spinal cord volume

that receives a PDT dose greater than the threshold dose required to induce spinal cord damage. By superimposing threshold dose contours onto the radiological images and comparing the actual dose received by the different anatomical structures, one can effectively determine the efficacy and safety for any given fiber placement (see below). In reality the optical environment within the tissue changes throughout the treatment and therefore so must the contour maps. Moreover, the biological response or threshold required for kill will also shift due to altered cellular metabolism and biochemistry, tissue blood flow, and oxygenation. Despite the influence of blood pooling we were able to demonstrate in porcine that 150 J/cm (150 mW/cm), 690-nm laser light 30 minutes after Verteporfin (6mg/m^2; i.v.) produces a mean radius of necrosis within bone marrow of 0.59 ±0.02 cm around the delivery fiber with a necrotic threshold of 9.3 J/cm^2 (4.3 mW/cm^2). A margin of apoptosis extending up to 2 cm out from the fiber was also evident histologically. As with previous reports in flat bone [29], we did not see any detrimental effects to the organic osteoid matrix. Indeed, prior biomechanical testing of rat vertebrae (unpublished results) confirms that PDT strengthens bone.

15.1.7 Treatment Planning

The vertebral anatomy in porcine is sufficiently similar to that of humans to provide a good model for testing a number of components specific to our treatment planning, including dosimetry, image-guided placement of optical fibers, and PDT response. Rigorous preoperative planning of the intended treatment protocol is fundamental to safety and efficacy. Treatment planning uses radiological images of the treatment site and interactive software tools to provide patient-specific prescriptions for optimized treatment. Primary components include (1) preoperative MRI/CT imaging and virtual planning, (2) intraoperative image-guidance/navigation, (3) real-time dosimetry of delivered dose with iterative adjustment to allow for changing optical properties, and (4) assessment of the biological response.

In practical terms the planning involves exporting preoperative axial CT DICOM images of target vertebra into a commercial virtual software, in our case, Mimics® software (9.0; Materialise, Ann Arbor, MI, USA), which allows segmentation of radiological images. Virtual objects, such as tumor or optical fiber, are then drawn into the vertebra. All features of the vertebra, including spinal canal, are anatomically accurate. Dose contours are projected into the virtual image using initial graph exchange specification format in order to determine the optimal fiber placement according to optical properties, PDT photosensitizer concentrations, and the sensitivities of the different tissue types to PDT (Figure 15.1). Once determined, the stereo-lithographic (STL) files of the target volume are exported into the online navigation system. The prescribed fiber position is defined in the same coordinate space as the pretreatment images, which are registered to the online navigation images through a series of fiducial markers placed onto the patient (see below). The surgeon therefore has a target to aim for when placing the actual treatment fiber. This approach is being used successfully in current clinical trials for treating prostate cancer [32]. Currently, online adjustment of delivered dose is conducted manually, although in theory biological sensors placed into the treatment zone would allow automatic feedback.

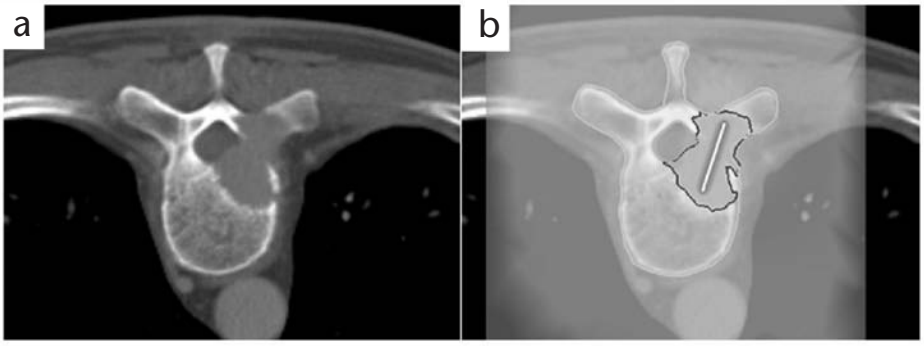

Figure 15.1 (a) CT image of target vertebra with virtual lesion embedded. (b) Fiber position within the vertebra can be optimized according to color contour maps overlaid onto the CT that show the PDT dose within the lesion and surrounding structures.

15.1.8 Image Guidance

Numerous imaging modalities, including magnetic resonance imaging, ultrasound, computer tomography (CT), and fluoroscopy, are being adapted to interventional procedures or being developed with image-guidance applications specifically in mind for surgery, interventional radiology, radiation therapy, and now photodynamic therapy. The goal is to improve the geometric precision of treatment (e.g., a scalpel, a laser, or a radiotherapeutic beam) and to move more toward minimally invasive procedures that can be conducted within diagnostic radiology. PDT in spine is no exception. Our group has developed a mobile cone beam CT [33] to provide superior guidance of optical fibers into vertebrae [34]. The current system combines an isocentric C-arm and PaxScan 4030A flat-panel detector (Varian Imaging Products, Palo Alto, CA) with servo drive for orbital motion (~178°) mounted onto a Siemens PowerMobil mobile allowing for large fields of view (15 cm axial length) and soft-tissue visualization both complimentary to its prospective use in image-guided surgery, interventional radiology, and percutaneous PDT (Figure 15.2). The detector offers real-time radiographic/fluoroscopic imaging, with rapid volume reconstruction (256×256×192) using the FDK algorithm [35]. Breakaway Imaging, LLC, (Littleton, MA) in partnership with Medtronic Inc., (Minneapolis, MN) has recently launched a new "O" arm with 360° orbital motion. A comparison to test the accuracy of cone beam CT versus conventional fluoroscopy has not been tested. For navigation we use a stereoscopic infrared camera (NDI Polaris) offering real-time acquisition (30 fps), large field of view (3 m^3; depth of field 1.5-3 m), and high resolution (0.4 mm). A handheld "wand" with CT-visible fiducials is then detected by the camera and assigned a set of coordinates that define its precise location in 3-D space. Using this system we have demonstrated the feasibility of placing 0.94-mm diameter (2.5-cm diffusing) optical fibers safely into the vertebral bodies of porcine and canines via bilateral transpedicular approach.

Canine vertebrae are denser than porcine; their pedicles also project more laterally, making transpedicular approach more difficult. Nevertheless, placement was possible and moderate (200 J/cm) or high-dose PDT (500 J/cm; 250 mW/cm) within T12 vertebra 5 minutes after Verteporfin infusion (0.4 mg/Kg) resulted in lesions

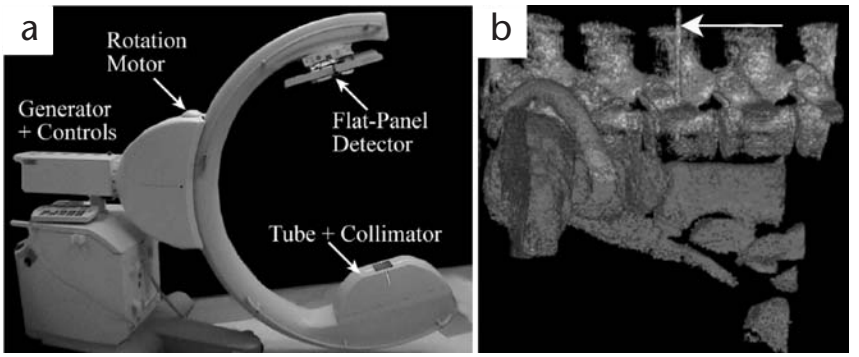

Figure 15.2 (a) A mobile cone beam CT with large, flat panel detector was used for placing fibers into the spine. (b) Rapid 3-D reconstructions of the spine and surrounding soft tissues allows for accurate intraoperative navigation.

within bone marrow and fat deposits averaging 1.1-cm diameter, slightly smaller than those in porcine [25]. MRI using contrast enhanced T1-weighted sequences provided valuable diagnostic assessment of damage at 7 days posttreatment that correlated well with histology. Enhanced signal was confined to a zone along the diffusing tip. Neurological evaluation of somato-sensory evoked potentials before, during, and after PDT confirmed sustained neurological function and standard analgesic administration provided good pain control such that animals were fully mobile the following morning after treatment. The rapid clearance of Verteporfin from blood within 30 to 60 minutes was marked by the lack of skin photosensitivity.

15.2 Photodynamic Therapy for Primary Osteosarcoma

Without a large animal model of spinal metastases with which to demonstrate efficacy, we opted to treat companion canines with large, high-grade (IIb) appendicular osteosarcoma as an alternative [36]. Seven large-breed canines with spontaneous osteosarcoma in their distal radius were MRI imaged prior to treatment. Tumors displayed necrotic centers with osteoid scarring throughout. A single 5-cm diffusing fiber was guided using fluoroscopy through the medullary cavity into the tumor. High-dose light (500 J/cm; 250 mW/cm) was delivered at 5 minutes post-Verteporfin infusion followed 48 hours later by MRI and limb amputation as part of the standard of care. Contrast-enhanced T1 sequences confirmed tumor ablation in all animals. Stereological examination revealed an average volume of effect of 14.96 cm^3 with mean medial to lateral dimensions of 3.4 cm and rostra-caudal dimensions of 5.51 cm (Color Plate 17). Importantly, similar volumes are reported for spinal lesions in clinic. Collectively this data provides definitive credence to the feasibility, efficacy, and safety of PDT treatment of lesions within the spine.

Of course it is inconceivable to assume that preclinical models can ever fully depict all of the clinical manifestations implicit to systemic disease and the practical issues of probe placement into critically ill patients with severely osteoporotic

bone will no doubt prove more challenging. The true test can only be conducted in clinical trials.

15.3 Antimicrobial PDT

Antimicrobial PDT is an emerging field with more than 100 scientific manuscripts listed under the www.pubmed.gov Web site in the past 2 years. However, less than one quarter of these pertain to biofilm. Photosensitizers commonly used include cationic phenothiazines, porphyrin derivatives, merocyanine 540, and 5-aminolevulinic acid (ALA) [37, 38]. None display complete specificity for bacteria, however, but rely on charge-mediated uptake or endogenous production (see below). A clinical formulation of the phenothiazine derivative, methylene blue, Urolene blue™ is currently administered orally as an antiseptic to treat urinary tract infections as well as methemoglobinaemia or as an antidote to cyanide poisoning.

15.3.1 Bone Infection

Inflammation of bone and bone marrow following microbial contamination can be life-threatening. Infections can spread systemically in blood or locally through soft tissue following trauma, burns, or peripheral vascular disease. Secondary disease is also an important consideration and the risk of contracting skeletal infection is thought to increase up to 1,000 times in patients with diabetes or sickle cell anemia [39]. Postoperative infection is perhaps the fastest emerging causes of acute osteomyelitis with more than one million new cases of hip replacement worldwide each year [40]. Orthopedic implantations and prosthetic devices are particularly susceptible to biofilm formation derived from *Staphylococcus aureus (S. aureus*) and *Pseudomonas Aeruginosa (P. aeruginosa)*. Both strains are facultative that develop thick glycocalyx biofilm that adhere very effectively to host tissues and metallic implants, including pins and screws and prosthetic hips and joints, creating an effective barrier to antimicrobials. Biofilms are found in approximately 65% of infected patients and are highly resistant to antibiotics [41]. They comprise glycoprotein matrix that house intercommunicating microbial communities with intervening water channels for transfer of nutrients and removal of waste [41], but little is known regarding their microenvironmental oxygenation.

15.3.2 Current Strategies

Treatment of osteomyelitis currently includes surgery and parenteral antibiotics, neither of which is conducive to combat the growing number of antibiotic-resistant bacterial strains or the inherent obstinacy of bacterial biofilms and the long-term management necessary for recurring infections. There are a considerable number of reports describing small animal models of osteomyelitis spanning 40 years of research. A number of studies describe novel strategies for delivering antibiotics using biodegradable implants or beads into rat tibia or spine [42]. A common theme to most of these studies is the inability to eradicate all of the infection or prevent recurrence particularly when treating established biofilm.

We recently reported the novel application of PDT to osteomyelitis using S. aureus-biofilm-laden K wires implanted into rat tibia [43]. Using a bioluminescent strain of S. aureus we demonstrated effective treatment of biofilms grown in vivo using ALA or methylene blue. High dose, acute regimens of PDT (75 J/cm^2) resulted in transient responses, which relapsed within 48 hours after treatment. In vitro studies provided the first evidence that metronomic PDT could provide better long-term management of bacterial growth than acute PDT. Metronomic regimens of low-dose drug delivery have been adopted for chemotherapy to minimize toxicity and our group recently introduced the concept for PDT to improve selective apoptosis of brain tumors [44]. ALA is a substrate involved in heme synthesis and is well suited for metronomic delivery, with low toxicity and the option of enteral or parenteral delivery. However, gram-positive bacteria produce the less active photosensitizer, coproporphyrin III instead of protoporphyrin IX [45]. Meanwhile gram-negative strains including P. aeruginosa produce protoporphyrin IX with little coproporphyrin III. Undoubtedly, the premise that rapidly dividing cells produce more endogenous photosensitizer cannot be applied to cells in biofilm, which are largely senescent. It remains, therefore, to be confirmed whether metronomic PDT with ALA displays similar promise for in vivo models of osteomyelitis as it appears to in vitro.

15.3.3 HOT-PDT

Concurrent with these studies has been our interest in combining PDT with hyperbaric oxygen therapy (HOT) or carbogen. There is a wealth of literature describing the benefits of HOT against bacteria and previous reports confirm improved treatment of cancer using PDT in combination with HOT [46, 47]. The physiological response of host tissues and resident bacteria to HOT is not clearly understood. Oxygen under normal atmospheric pressure is poorly absorbed into tissues. HOT can facilitate improved oxygenation of tissues, improved blood flow into infected sites, and ultimately improved access for drug delivery, which may explain the synergistic effect with antibiotics [48]. Oxidative stress is likely a primary mediator, which may also involve an immunological component although the precise interaction is unclear. Bacteria are well adapted to cope with oxidative stress. *S. aureus*, despite lacking glutathione, and contain a family of small soluble proteins called thioredoxins encoded by *trxA* and *trxB* genes that catalyze thiol-redox reactions. TrxA and trxB are activated in response to increased thiol oxidation and disulfide bond formation promoting thioredoxin reductase-mediated quenching of reactive oxygen species in the presence of NADPH [49, 50]. P. aeruginosa meanwhile relies on catalase as well as manganese- and iron cofactored superoxide dismutases encoded by *SodA* and *SodB* genes to combat oxidative stress. Nevertheless, tumor cells like bacteria also have effective defenses against oxidative stress yet remain highly susceptible to PDT-mediated cell kill and the additional molecular oxygen proffered by HOT should enhance singlet oxygen production within the cells, although direct measurements of singlet oxygen production during HOTPDT have not been carried out thus far. So far our observations in vitro confirm that combining HOT with acute PDT using 10 J/cm^2 and methylene blue can decrease the number of surviving S. aureus colonies by >2 $\log_{10}$ compared with PDT

alone (61). Importantly, a similar increase in antimicrobial action was also confirmed against S. aureus biofilms using methylene blue. Recent unpublished results from our group suggest an even greater improvement combining metronomic regimens of PDT and HOT. It will be imperative for future research to discern the underlying mechanism(s) related to the improved cell kill with HOT and perhaps quantify singlet oxygen production within biofilms directly.

15.4 Bone Growth Modulation

As we grow, our cartilaginous template is replaced with bone through a process called endochondral ossification. This process normally occurs in limbs around the chronological ages of 16 in males and 14 in females. In this process mesenchymal cells within the avascular growth plate (physis) condense and mature as chondroprogenitor cells into the proliferative zone. Extracellular matrix is laid down as chondrocytes exit their proliferative phase and terminally differentiate into hypertrophic chondrocytes. The matrix provides a scaffold for vascular invasion into the physis from the adjacent metaphysis and with this newly established blood flow come preosteoblasts and mesenchymal cells that contribute to calcification of the matrix and apoptosis of the matured chondrocytes [51, 52]. Once the transition from cartilage to bone is complete closure of the physis results in growth arrest. The whole process is tightly choreographed by hypoxia-inducible factor (HIF-1α), vascular endothelial growth factor-A isoforms ($VEGF_{164}$, $VEGF_{188}$) and receptor (VEGFR1), fibroblast growth factors (FGF-2, FGF-9, FGF-18) and receptor (FGFR-3), matrix metalloproteinases (MMP-9, MMP-13), p57, bone morphogenic proteins, B-cell lymphoma-2 (bcl-2), and parathyroid hormone-related peptide [52, 53]. Disruption of this process can lead to bone growth anomalies such as limb length discrepancy (LLD) or scoliosis. Realizing that the hypoxic gradient within the physis is governing to the process of angiogenesis and bone formation we hypothesized that vascular-targeted photodynamic therapy may be able to amplify this hypoxic gradient by destroying existing vasculature outside the physis and by doing so induce proangiogenic factors like VEGF-A to accelerate the onset of ossification [54, 55]. In other words, we set out to exploit the angiogenic response following PDT as a minimally invasive, fiber-optic-based procedure to modulate bone growth [56]. This raises new and exciting possibilities of using PDT to model and potentially treat LLD or scoliosis since current approaches, including surgical osteotomy, fixation, transphyseal screw placement, or stapling are associated with serious complications related to malunion, nonunion, axial rotation infection, and protracted pain or immobility [57, 58].

To quantify the induction of VEGF-A gene following PDT in growth plates we conducted studies using immature transgenic mice that constitutively express the luciferase gene. In these mice luciferase activity is induced by a transcriptional promoter sequence specific to VEGF-A. Activation of VEGF within localized tissues results in a corresponding luciferase-mediated bioluminescence. Femoral and tibial growth plates were targeted for treatment using a 0.2-mm diameter optical fiber placed percutaneously onto the medial aspect of the lower limb facing laterally and held using a custom jig [56]. Light of varying dose was delivered 10 minutes follow-

ing intravenous injection of Verteporfin to ensure vascular-targeted response [59]. A repeat dose (x2) of 10 J (50 mW output) given 3 days apart provided the most consistent calcification or closure of growth plates resulting in pronounced VEGF-mediated angiogenesis and limb growth arrest (Color Plate 18). As mice grew, the discrepancy between treated and untreated limbs averaged 9.5% ± 4.4% by 4 weeks posttreatment.

Effects were very much light dose-dependent with exaggerated limb shortening; >20% with 27J, which resulted in fracture and pronounced thickening of the growth plate following lower doses of 5 or 10J in the absence of photosensitizer. The latter observation is of particular interest as this raises the possibility of not only shortening but also lengthening limbs, although studies to substantiate this have not been completed. The significance of this become clear when we consider the current options for limb lengthening involving distraction histiogenesis and external fixation that come with formidable risks of misalignment, nonunion, nerve palsy, excruciating pain, and prolonged convalescence [60]. The psychological morbidity and financial burden to patient and government can be considerable in these cases.

A similar rationale can be applied to scoliosis, the treatment for which often requires extensive surgery resulting in placement of steel rods along length of the spine, permanently fixing the spine. There are numerous reports describing preclinical models of scoliosis such as pinealized chicken or amputation of limbs or transverse processes [61, 62]. While these do well to mimic the morphological presentation of scoliosis they offer little as to the underlying etiology and in most cases do not agree with what is currently known about the genetic predisposition of patients to idiopathic scoliosis (82). It should be noted, however, that pinealectomy reduces melatonin levels and a number of scoliosis patients with intact pineal glands have presented with reduced melatonin. Finally, melatonin is known to inhibit VEGF, so reduced levels of melatonin would tend to increase VEGF levels in a similar fashion to calmodulin, which has also been shown to be elevated in scoliosis patients [63]. These findings strengthen the argument for an angiogenic component to scoliosis.

In the early 1960s, scientists first began to investigate the preponderance of scoliosis occurring in thoracic spine and the vascular discrepancy that was known to exist between left and right sides [64]. It was concluded that disparity in the vascular supply between left and right spine during the growth period could be underlying to the etiology of scoliosis. Subsequent animal studies supported these initial hypotheses [65–67]. It is clear that if one side of the spine grows faster than the other curvature may result as wedging of the vertebrae create convexity or kyphotic curve. 3-dimensional complexity of curve may evolve as vertebrae, which possess two growth plates—one providing expansion through the rostra-caudal plane, and the other the neural central cartilage—sat dorsolaterally to the pedicles providing expansion in the axial plane [68]. An extension of this would be to suppose that like limbs, the spine might be subject to asymmetrical closure of growth plates secondary to hypoxic stress-mediated vascularization. Interestingly, in our preliminary, experiments we have demonstrated the ability to produce a modest 5° to 8° scoliotic curve in a number of mice following unilateral treatment in the lumbar spine (L1, L2) of transgenic mice (Color Plate 19). Closure to one side of the growth

plate was confirmed histologically and microcomputed tomography revealed structural damage. An interesting side to this data was the histological changes to intervertebral discs. In a number of animals discs appeared to be expanded with increasing numbers of fibro-cartilaginous rings of the annulus fibrosis and notable loss of the nucleus pulposus. Immunohistochemistry revealed increased VEGF staining throughout the annulus fibrosis. The significance of this data and whether it mimics any of the histological changes evident in degenerative disc disease remains to be confirmed.

Currently, our studies do suggest a role for vascular anomaly in LLD and scoliosis and suggest that PDT is a valuable method for preclinical modeling of these conditions.

15.5 Conclusion

The application of PDT in bone opens a number of very interesting and potentially clinically important avenues for investigation. The ability to plan prior to surgery where to deliver the light in order to achieve the best possible treatment of the cancer without damaging neighboring structures, and to then execute that plan with the utmost accuracy using online navigation in the operating suite offers the kind of reassurance that clinicians must have when operating in the spine, and will go a long way in promoting clinical treatment of spinal metastases using PDT.

Osteomyelitis is a significant risk following surgery and patients with advanced stage cancers far worse than most in their ability to fight infection or endure surgical debridment or prolonged exposure to antibiotics. The potential for targeting both infection and cancer minimally invasively using PDT and perhaps even using the same photosensitizer is certainly appealing; however, it is likely that the optimal treatment regimen will differ for each ailment. The opportunity for using implantable devices that allow metronomic PDT delivery could prove highly effective against recurring infections assuming the infection has access to molecular oxygen to allow singlet oxygen generation. The same may also be true for cancers. The development of metronomic PDT for treating cancer, meanwhile, offers tremendous potential and is currently under preclinical and clinical investigation for brain cancers. Bacterial biofilms offer a particular challenge providing an effective barrier to antibiotics and photosensitizers alike, as well as to nutrients and oxygen, which will limit the photodynamic action of any photosensitizer relying on type II photooxidation. Results combining hyperbaric oxygen therapy and PDT are compelling and raise the possibility of improving PDT efficacy in poorly oxygenated infections. Nevertheless, for antimicrobial PDT to gain wider acceptance among clinicians, it is clear that new photosensitizers will have to be designed that offer improved targeting and accumulation inside bacterial cells and biofilms. Given the impending pandemic that may result as more strains become resistant to antibiotics, the pursuit of alternate strategies for treating infection should be considered one of the most important biomedical pursuits in science today. The versatility and specificity of PDT regards dosing and delivery may provide a far superior treatment and management of infection than antibiotics and minimize the risk of developing resistance as well as collateral damage to host bacteria.

Bone is a dynamic tissue, constantly changing and growing, and in the case of cancellous bone, highly conducive to the transmittance of light. The capacity to modulate bone growth using PDT toward a therapeutic end has never to our knowledge been described before. The fact that we can model limb growth arrest and create curves in the spines of rodents using PDT should allow greater understanding as to the roles of aberrant hypoxia and angiogenesis in premature growth plate closure and perhaps provide a means of correcting such anomalies without the need for painful invasive surgeries. It seems almost fitting that PDT-induced angiogenesis, while instrumental to the flurry of recent research combining anti-VEGF and PDT for treating age-related macular degeneration, should now perhaps be exploitable for another therapy. Of additional interest is the possibility that we can modulate the growth plate to expand prior to closure, thereby lengthening the bone. This would represent a major contribution to orthopedics and to the scientific community at large, galvanizing the acceptance of modern science and biophotonics into clinic.

Acknowledgments

I would like to acknowledge Drs. Shane Burch, Albert Yee, Brian Wilson, and Jeffery Siewerdsen, who are integral contributors to the ongoing research and clinical expertise related to PDT in bone here at the University Health Network in Toronto, Canada. I also wish to thank Crystal Johnson and Claudia Chien, who helped with much of the work described in this chapter.

References

[1] Walsh, G. L., et al., "Anterior approaches to the thoracic spine in patients with cancer: indications and results," *Ann Thorac Surg*, Vol. 64, 1997, pp. 1611–1618.

[2] Tatsui, H., et al., "Survival rates of patients with metastatic spinal cancer after scintigraphic detection of abnormal radioactive accumulation," *Spine*, Vol. 21, 1996, pp. 2143–2148.

[3] Bauer, H. C., and Wedin, R., "Survival after surgery for spinal and extremity metastases. Prognostication in 241 patients," *Acta Orthop Scand*, Vol. 66, 1995, pp. 143–146.

[4] Hirabayashi, H., et al., "Clinical outcome and survival after palliative surgery for spinal metastases: palliative surgery in spinal metastases," *Cancer*, Vol. 97, 2003, pp. 476–484.

[5] Klimo, P., Jr., and Schmidt, M. H., "Surgical management of spinal metastases," *Oncologist*, Vol. 9, 2004, pp. 188–196.

[6] Mercadante, S., "Malignant bone pain: pathophysiology and treatment," *Pain*, Vol. 69, 1997, pp. 1–18.

[7] Zaidat, O. O., and Ruff, R. L., "Treatment of spinal epidural metastasis improves patient survival and functional state," *Neurology*, Vol. 58, 2002, pp. 1360–1366.

[8] De Leenheer, E., et al., "Evidence of a role for RANKL in the development of myeloma bone disease," *Curr Opin Pharmacol*, Vol. 4, 2004, pp. 340–346.

[9] Hofbauer, L. C., and Schoppet, M., "Clinical implications of the osteoprotegerin/RANKL/RANK system for bone and vascular diseases," *Jama*, Vol. 292, 2004, pp. 490–495.

[10] Hormbrey, E., et al., "The relationship of human wound vascular endothelial growth factor (VEGF) after breast cancer surgery to circulating VEGF and angiogenesis," *Clin Cancer Res*, Vol. 9, 2003, pp. 4332–4339.

[11] Rajesh, L., et al., "Correlation between VEGF expression and angiogenesis in breast carcinoma," *Anal Quant Cytol Histol*, Vol. 26, 2004, pp. 105–108.

[12] Schoppet, M., Preissner, K. T., and Hofbauer, L. C., "RANK ligand and osteoprotegerin: paracrine regulators of bone metabolism and vascular function," *Arterioscler Thromb Vasc Biol*, Vol. 22, 2002, pp. 549–553.

[13] Carteni, G., et al., "Efficacy and safety of zoledronic acid in patients with breast cancer metastatic to bone: a multicenter clinical trial," *Oncologist*, Vol. 11, 2006, pp. 841–848.

[14] Faul, C. M., and Flickinger, J. C., "The use of radiation in the management of spinal metastases," *J Neurooncol*, Vol. 23, 1995, pp. 149–161.

[15] Ferris, F. D., Bezjak, A., and Rosenthal, S. G., "The palliative uses of radiation therapy in surgical oncology patients," *Surg Oncol Clin N Am*, Vol. 10, 2001, pp. 185–201.

[16] Ghogawala, Z., Mansfield, F. L., and Borges, L. F., "Spinal radiation before surgical decompression adversely affects outcomes of surgery for symptomatic metastatic spinal cord compression," *Spine*, Vol. 26, 2001, pp. 818–824.

[17] Tombolini, V., et al., "Radiation therapy of spinal metastases: results with different fractionations," *Tumori*, Vol. 80, 1994, pp. 353–356.

[18] Chow, E., et al., "Radiotherapeutic approaches to metastatic disease," *World J Urol*, Vol. 21, 2003, pp. 229–242.

[19] Ryu, S., et al., "Patterns of failure after single-dose radiosurgery for spinal metastasis," *J Neurosurg*, Vol. 101 Suppl 3, 2004, pp. 402–405.

[20] Mang, T. S., et al., "A phase II/III clinical study of tin ethyl etiopurpurin (Purlytin)-induced photodynamic therapy for the treatment of recurrent cutaneous metastatic breast cancer," *Cancer J Sci Am*, Vol. 4, 1998, pp. 378–384.

[21] Nathan, T. R., et al., "Photodynamic therapy for prostate cancer recurrence after radiotherapy: a phase I study," *J Urol*, Vol. 168, 2002, pp. 1427–1432.

[22] Engebraaten, O., and Fodstad, O., "Site-specific experimental metastasis patterns of two human breast cancer cell lines in nude rats," *Int J Cancer*, Vol. 82, 1999, pp. 219–225.

[23] Burch, S., et al., "Photodynamic therapy for the treatment of vertebral metastases in a rat model of human breast carcinoma," *J Orthop Res*, Vol. 23, 2005, pp. 995–1003.

[24] Burch, S., et al., "Multimodality Imaging for Vertebral Metastases in a Rat Osteolytic Model," *Clin Orthop Relat Res*, Vol. 454, 2007, pp. 230–236.

[25] Burch, S., et al., "Photodynamic therapy for the treatment of metastatic lesions in bone: studies in rat and porcine models," *J Biomed Opt*, Vol. 10, 2005, pp. 034011.

[26] Farrar, S. K., et al., "Optical properties of human trabecular meshwork in the visible and near-infrared region," *Lasers Surg Med*, Vol. 25, 1999, pp. 348–362.

[27] Firbank, M., et al., "Measurement of the optical properties of the skull in the wavelength range 650–950 nm," *Phys Med Biol*, Vol. 38, 1993, pp. 503–510.

[28] Flock, S. T., Wilson, B. C., and Patterson, M. S., "Monte Carlo modeling of light propagation in highly scattering tissues—II: Comparison with measurements in phantoms," *IEEE Trans Biomed Eng*, Vol. 36, 1989, pp. 1169–1173.

[29] Tauber, S., et al., "Lightdosimetric quantitative analysis of the human petrous bone: experimental study for laser irradiation of the cochlea," *Lasers Surg Med*, Vol. 28, 2001, pp. 18–26.

[30] Cerussi, A., et al., "In vivo absorption, scattering, and physiologic properties of 58 malignant breast tumors determined by broadband diffuse optical spectroscopy," *J Biomed Opt*, Vol. 11, 2006, pp. 044005.

[31] Jacques, S. L., "Light distributions from point, line and plane sources for photochemical reactions and fluorescence in turbid biological tissues. [Review] [22 refs]," *Photochem Photobiol*, Vol. 67, 1998, pp. 23–32.

[32] Weersink, R. A., et al., "Techniques for delivery and monitoring of TOOKAD (WST09)-mediated photodynamic therapy of the prostate: clinical experience and practicalities," *J Photochem Photobiol B*, Vol. 79, 2005, pp. 211–222.

[33] Rafferty, M. A., et al., "Intraoperative cone-beam CT for guidance of temporal bone surgery," *Otolaryngol Head Neck Surg*, Vol. 134, 2006, pp. 801–808.

[34] Siewerdsen, J. H., et al., "Volume CT with a flat-panel detector on a mobile, isocentric C-arm: pre-clinical investigation in guidance of minimally invasive surgery," *Med Phys*, Vol. 32, 2005, pp. 241–254.

[35] Defrise, M., Townsend, D. W., and Clack, R., "Three-dimensional image reconstruction from complete projections," *Phys Med Biol*, Vol. 34, 1989, pp. 573–587.

[36] Burch, S., et al., "Multimodality imaging strategies for vertebral metastases in a preclinical osteolytic model," submitted, Vol., 2007.

[37] Hamblin, M. R., and Hasan, T., "Photodynamic therapy: a new antimicrobial approach to infectious disease?" Vol. 3, 2004, pp. 436–450.

[38] Jori, G., et al., "Photodynamic therapy in the treatment of microbial infections: Basic principles and perspective applications," *Lasers Surg Med*, Vol. 38, 2006, pp. 468–481.

[39] Epps, C. H., Jr., et al., "Osteomyelitis in patients who have sickle-cell disease. Diagnosis and management," *J Bone Joint Surg Am*, Vol. 73, 1991, pp. 1281–1294.

[40] Fisman, D. N., et al., "Clinical effectiveness and cost-effectiveness of 2 management strategies for infected total hip arthroplasty in the elderly," *Clin Infect Dis*, Vol. 32, 2001, pp. 419–430.

[41] O'Connell, H. A., et al., "Influences of biofilm structure and antibiotic resistance mechanisms on indirect pathogenicity in a model polymicrobial biofilm," *Appl Environ Microbiol*, Vol. 72, 2006, pp. 5013–5019.

[42] An, Y. H., Kang, Q. K., and Arciola, C. R., "Animal models of osteomyelitis," *Int J Artif Organs*, Vol. 29, 2006, pp. 407–420.

[43] Bisland, S. K., et al., "Pre-clinical in vitro and in vivo studies to examine the potential use of photodynamic therapy in the treatment of osteomyelitis," *Photochem Photobiol Sci*, Vol. 5, 2006, pp. 31–38.

[44] Bisland, S. K., et al., "Metronomic photodynamic therapy as a new paradigm for photodynamic therapy: rationale and preclinical evaluation of technical feasibility for treating malignant brain tumors," *Photochem Photobiol*, Vol. 80, 2004, pp. 22–30.

[45] Nitzan, Y., et al., "ALA induced photodynamic effects on gram positive and negative bacteria," Vol. 3, 2004, pp. 430–435.

[46] Huang, Z., et al., "Hyperoxygenation enhances the tumor cell killing of photofrin-mediated photodynamic therapy," *Photochem Photobiol*, Vol. 78, 2003, pp. 496–502.

[47] Maier, A., et al., "Combined photodynamic therapy and hyperbaric oxygenation in carcinoma of the esophagus and the esophago-gastric junction," *Eur J Cardiothorac Surg*, Vol. 18, 2000, pp. 649–654; discussion 654–645.

[48] Mendel, V., Simanowski, H. J., and Scholz, H., "Synergy of HBO2 and a local antibiotic carrier for experimental osteomyelitis due to Staphylococcus aureus in rats," *Undersea Hyperb Med*, Vol. 31, 2004, pp. 407–416.

[49] Arner, E. S., and Holmgren, A., "Physiological functions of thioredoxin and thioredoxin reductase," *Eur J Biochem*, Vol. 267, 2000, pp. 6102–6109.

[50] Uziel, O., et al., "Transcriptional regulation of the Staphylococcus aureus thioredoxin and thioredoxin reductase genes in response to oxygen and disulfide stress," *J Bacteriol*, Vol. 186, 2004, pp. 326–334.

[51] Goldring, M. B., Tsuchimochi, K., and Ijiri, K., "The control of chondrogenesis," *J Cell Biochem*, Vol. 97, 2006, pp. 33–44.

[52] Kronenberg, H. M., "Developmental regulation of the growth plate," *Nature*, Vol. 423, 2003, pp. 332–336.

[53] Schipani, E., et al., "Hypoxia in cartilage: HIF-1alpha is essential for chondrocyte growth arrest and survival," *Genes Dev*, Vol. 15, 2001, pp. 2865–2876.

[54] Maes, C., et al., "Impaired angiogenesis and endochondral bone formation in mice lacking the vascular endothelial growth factor isoforms VEGF164 and VEGF188," *Mech Dev*, Vol. 111, 2002, pp. 61–73.

[55] Maes, C., et al., "Soluble VEGF isoforms are essential for establishing epiphyseal vascularization and regulating chondrocyte development and survival," *J Clin Invest*, Vol. 113, 2004, pp. 188–199.

[56] Bisland, S. K., et al., "A new technique for physiodesis using photodynamic therapy," *Clin Orthop Relat Res*, Vol. 461, 2007, pp. 153–161.

[57] Horton, G. A., and Olney, B. W., "Epiphysiodesis of the lower extremity: results of the percutaneous technique," *J Pediatr Orthop*, Vol. 16, 1996, pp. 180–182.

[58] Nouth, F., and Kuo, L. A., "Percutaneous epiphysiodesis using transphyseal screws (PETS): prospective case study and review," *J Pediatr Orthop*, Vol. 24, 2004, pp. 721–725.

[59] Bisland, S. K., et al., "A rationale for treating leg length discrepancy using photodynamic therapy," *Proc SPIE*, Vol. 5969, 2005, pp. 258–266.

[60] Aaron, A. D., and Eilert, R. E., "Results of the Wagner and Ilizarov methods of limb-lengthening," *J Bone Joint Surg Am*, Vol. 78, 1996, pp. 20–29.

[61] Machida, M., et al., "Pathologic mechanism of experimental scoliosis in pinealectomized chickens," *Spine*, Vol. 26, 2001, pp. E385–391.

[62] Thomas, S., and Dave, P. K., "Experimental scoliosis in monkeys," *Acta Orthop Scand*, Vol. 56, 1985, pp. 43–46.

[63] Cheng, J. C., et al., "Osteopenia in adolescent idiopathic scoliosis: a histomorphometric study," *Spine*, Vol. 26, 2001, pp. E19–23.

[64] Brodetti, A., and Cauchoix, J., "The vascular supply of the spine of normal and lathyric rabbits in relation to the pathogenesis of experimental scoliosis," *Clin Orthop*, Vol. 25, 1962, pp. 180–203.

[65] Crock, H. V., "The arterial supply and venous drainage of the vertebral column of the dog," *J Anat*, Vol. 94, 1960, pp. 88–99.

[66] Crock, H. V., and Goldwasser, M., "Anatomic studies of the circulation in the region of the vertebral end-plate in adult Greyhound dogs," *Spine*, Vol. 9, 1984, pp. 702–706.

[67] Crock, H. V., and Yoshizawa, H., "The blood supply of the lumbar vertebral column," *Clin Orthop Relat Res*, Vol., 1976, pp. 6–21.

[68] De Salis, J., Beguiristain, J. L., and Canadell, J., "The production of experimental scoliosis by selective arterial ablation," *Int Orthop*, Vol. 3, 1980, pp. 311–315.